Influence of Surface Heterogeneity on Electrokinetically Driven Microfluidic Mixing

David Erickson and Dongqing Li*

Department of Mechanical & Industrial Engineering, University of Toronto, 5 King's College Road, Toronto, Ontario, Canada M5S 3G8

Received October 23, 2001. In Final Form: December 7, 2001

Electroosmotic flow in microfluidic systems is limited to the low Reynolds number regime. As a result species mixing in electroosmotic flow systems is inherently diffusion dominated, requiring both a long mixing channel and retention time to attain a homogeneous solution. Recent studies have shown that the introduction of oppositely charged surface heterogeneities to microchannel walls can result in regions of localized flow circulation within the bulk flow. In this study we seek to investigate these circulation regions, through 3D finite-element based numerical simulations, and then use them as a method of enhancing species mixing in a T-shaped micromixer. While all cases of surface heterogeneity are shown to enhance mixing efficiency, greater improvement is found when both the size of the heterogeneous region and the degree of heterogeneity (i.e., the difference between the heterogeneous and homogeneous ζ-potentials) are increased. In some cases the presence of heterogeneous regions is shown to reduce the required mixing channel length by as much as 70%.

I. Introduction

Recent interest in electrokinetic flow over heterogeneous surfaces originated with the pioneering studies of Norde et al.[1] and others[2−4] who used the streaming potential technique as a tool for the study of protein adsorption onto various materials. Since then a number of theoretical and numerical models[5,6] have been developed to predict electrokinetic effects resulting from pressure-driven flow over heterogeneous surfaces.

Less well studied are the effects of surface heterogeneity on electroosmotically induced flow. Recently Ajdari[7] presented a theoretical treatment for this case and suggested that the presence of heterogeneous regions with a net surface charge density of opposite sign to that of the homogeneous surface (or equivalently a ζ-potential of opposite sign) can result in the circulation regions within the bulk flow near these heterogeneous patches. This behavior was later observed in slit microchannels experimentally by Stroock et al.,[8] who found excellent agreement with their flow model.

The production of these bulk flow circulation regions can be explained by considering a simple model illustrated in Figure 1. In this figure, electroosmotically induced flow over a homogeneous surface with a zeta potential $\zeta = -|\zeta_o|$ is compared with that for a surface with an oppositely charged heterogeneous patch characterized by $\zeta = +|\zeta_o|$. For the homogeneous case (Figure 1a) the electroosmotic body force applied to the liquid continua within the double layer is equivalent at each point along the flow axis and results in a constant bulk liquid velocity at the edge of the diffuse double layer, v_{eo}, which can be described by[9]

$$v_{eo} = \mu_{eo}\nabla\phi = \left(\frac{\epsilon_w\zeta}{\eta}\right)\nabla\phi \tag{1}$$

where μ_{eo} is the electroosmotic mobility, ϵ_w is the electrical permittivity of the solution, η is the viscosity, and ϕ is the applied electric field strength. The same relation holds true for the heterogeneous surface in Figure 1b except the electroosmotic body force is now applied to a region with excess negative ions and thus is in the opposite direction to that in the homogeneous regions. The interaction of these local flow fields with the bulk flow results in the regional circulation zones, as is illustrated in Figure 1b.

Our interest in electroosmotic flow over heterogeneous surfaces can be attributed to two factors. First, the advancement of micromanufacturing technology has made possible the development of a variety of complex microscale surface charge patterns (see Stroock et al.[8] for an example). Second, electrokinetic flow is widely used as a primary method of species transport in a number of biological and chemical analysis systems.[10] In this study we consider a simple T-shaped microfluidic mixing system, as shown in Figure 2. This simple arrangement has been used for numerous applications including the dilution of a sample in a buffer,[11] the development of complex species gradients,[12−13] and measurement of the diffusion coefficient.[14] In addition the T-sensor has also been exploited to make diagnostic determinations of analyte concentra-

* To whom correspondence may be addressed. E-mail: dli@mie.utoronto.ca. Fax: (416) 978-7753.

(1) Norde, W.; E. Rouwendal, E. *J. Colloid Interface Sci.* **1990**, *139*, 169−176.
(2) Elgersma, A. V.; Zsom, R. L. J.; Lyklema, J.; Norde, W. *Colloid Surf.* **1992**, *65*, 17−28.
(3) Zembala, M.; Déjardin, P. *Colloid Surf., B* **1994**, *3*, 119−129.
(4) Werner, C.; Jacobasch, H. J. *Macromol. Symp.* **1996**, *103*, 43−54.
(5) Adamczyk, Z.; Warszynzki, P.; Zembala, M. *Bull. Pol. Acad. Sci. Chem.* **1999**, *47* (3), 239−258.
(6) Erickson, D.; Li, D. *J. Colloid Interface Sci.* **2001**, *237*, 283−289.
(7) Ajdari, A. *Phys. Rev. Lett.* **1995**, *75* (4), 755−758.
(8) Stroock, A. D.; Weck, M.; Chiu, D. T.; Huck, W. T. S.; Kenis, P. J. A.; Ismagilov, R. F.; Whitesides, G. M. *Phys. Rev. Lett.* **2000**, *84* (15), 3314−3317. Also see Stroock, A. D.; Weck, M.; Chiu, D. T.; Huck, W. T. S.; Kenis, P. J. A.; Ismagilov, R. F.; Whitesides, G. M. *Phys. Rev. Lett.* **2001**, *86* (26), 6050.
(9) Hunter, R. J. *Zeta Potential in Colloid Science*; Academic Press: London, 1981.
(10) Krishnan, M.; Namasivayam V.; Lin, R.; Pal, R.; Burns, M. *Curr. Opin. Biotechnol.* **2001**, *12*, 92−98.
(11) Harrison J. D.; Fluri, K.; Seiler, K.; Fan, Z.; Effenhauser, C.; Manz, A. *Science* **1993**, *261*, 895−897.

10.1021/la015646z CCC: $22.00
Published on Web 02/01/2002

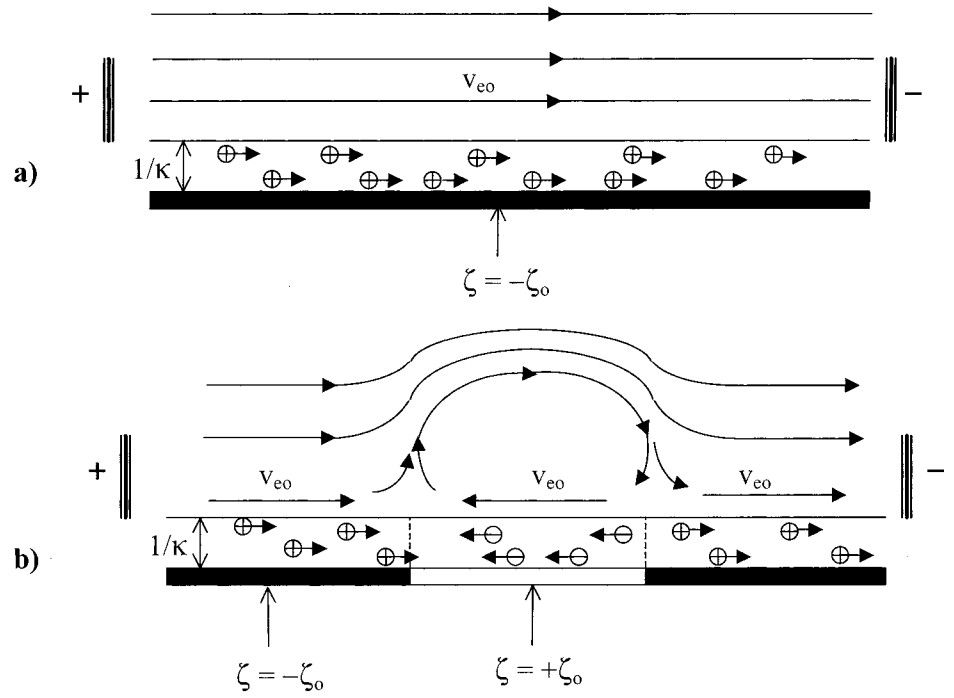

Figure 1. Electroosmotic flow near the double layer region for (a) a homogeneous surface ($\zeta = -|\zeta_o|$) and (b) a homogeneous surface with a heterogeneous patch ($\zeta = +|\zeta_o|$). Over the heterogeneous patch, the excess cations are attracted to the positive electrode resulting in an electroosmotic flow in the opposite direction to that over the homogeneous regions with an excess anion concentration. Arrows represent streamlines and $1/\kappa$ refers to the characteristic thickness of the electrical double layer.

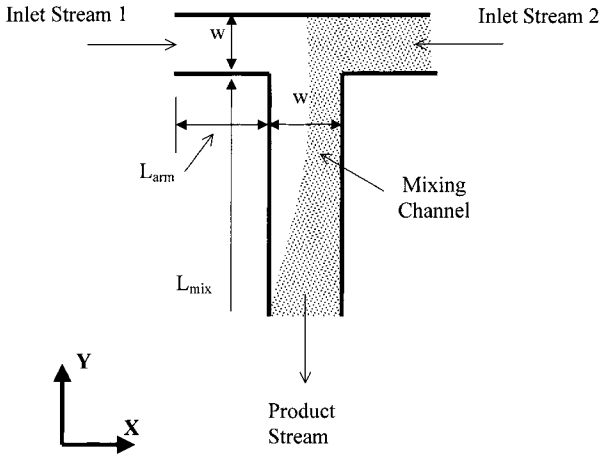

Figure 2. T-shaped micromixer formed by the intersection of two microchannels, showing a schematic of the mixing/dilution process.

tions[15] by introducing the analyte of interest in one stream to a receptor molecule in the other (e.g., a pH[16] or flouresence[17] indicator) producing a measurable signal which can be related to the parameter of interest.[14]

In general most microfluidic mixing systems, whether pressure or electrokinetically driven, are limited to the low Reynolds number regime, and thus species mixing is strongly diffusion dominated, as opposed to convection or turbulence dominated at higher Reynolds numbers. Consequently mixing tends to be slow and occur over relatively long distances and time. As an example the concentration gradient generator presented by Dertinger et al.[12] required a mixing channel length on the order of 9.25 mm for a 45 μm × 45 μm cross sectional channel or approximately 200 times the channel width to achieve nearly complete mixing.

The purpose of this study is to examine the fundamental influence of surface heterogeneity on the flow and species mixing in electroosmotically driven microfluidic devices, through the use of 3D numerical flow simulations. A variety of patch configurations, ζ-potentials, electric field strengths, and channel sizes will be examined with the goal of determining the optimum conditions for enhanced mixing. To our knowledge this is the first study to investigate enhanced mixing in microfluidic systems through the introduction of heterogeneous surfaces patches.

II. Modeling Details

In a number of recent studies computational fluid dynamics modeling has proven to be an excellent tool for analyzing electrokinetic flow in microfluidic systems and devices. In their work Ermakov et al.[18] used a 2D code to model electrokinetic focusing in a microchannel and species mixing at a T-shaped intersection. The results of their computations were shown to be in excellent agreement with experimental results. Bianchi et al.[19] presented finite element-based simulations of combined electroosmotic and pressure-driven flow at a T-intersection. 3D flow simulations were presented by Patankar et al.[20] who examined the flow behavior at a cross intersection. In

(12) Dertinger, S. K. W.; Chiu, D. T.; Jeon, N. L.; Whitesides, G. M. *Anal. Chem.* **2001**, *73*, 1240−1246.
(13) Jeon, N. L.; Dertinger, S. K. W.; Chiu, D. T.; Choi, I. S.; Stroock, A. D., Whitesides, G. M. *Langmuir* **2000**, *16*, 8311−8316.
(14) Kamholz, A. E.; Schiling, E. A.; Yager, P. *Biophys. J.* **2001**, *80*, 1967−1972.
(15) Weigl, B.; Yager, P. *Science* **1999**, *283*, 346−347.
(16) Galambos, P.; Forster, F. K.; Weigl, B. *Proceedings of the international conference on solid-state sensors and actuators*; IEEE: Piscataway, NJ, 1997.
(17) Kamholz, A. E.; Weigl, G. H.; Finlayson, B. A.; Yager, P. *Anal. Chem.* **1999**, *71*, 5340−5347.
(18) Ermakov, S. V.; Jacobson, S. C.; Ramsey, J. M. *Anal. Chem.* **1998**, *70*, 4494−4504.
(19) Bianchi, F.; Ferrigno, R.; Girault, H. H. *Anal. Chem.* **2000**, *72*, 1987−1993.
(20) Patankar, N. A.; Hu, H. H. *Anal. Chem.* **1998**, *70*, 1870−1881.

another recent study Erickson and Li[21] used 3D thermal simulations to develop an optimized microfluidic device for PCR-based DNA amplification. To date however this will be the first study to present full 3D simulations of electrokinetic circulation in microfluidic devices and its potential effects on enhanced species mixing. The theoretical considerations pertaining to the modeling of electroosmotic flow in microchannels have been covered in detail by both Ermakov et al.[18] and Patankar et al.[20] and thus here we concentrate primarily on presenting the relevant equations, primary assumptions, simulation conditions, and numerical method.

A. Basic Equations and Modeling Assumptions. Electroosmotic flow results from the interaction of an applied electric field with the unbalanced ion concentrations in the electrical double layer (EDL) and is described by the Navier−Stokes equations subject to an electroosmotic body force and the continuity equation (given below in nondimensional form)

$$Re\left[\frac{\partial V}{\partial \tau} + (V\cdot\tilde{\nabla})V\right] = -\tilde{\nabla}P + \tilde{\nabla}^2 V + F_e \qquad (2a)$$

$$\tilde{\nabla}\cdot V = 0 \qquad (2b)$$

where V is the nondimensional velocity ($V = v/v_{eo}$, where v_{eo} is calculated using eq 1), P is the nondimensional pressure, τ is the nondimensional time, and Re is the Reynolds number given by $Re = \rho v_{eo} L/\eta$, where L is a length scale taken as the channel width (w from Figure 2) in this case. In general the high voltage requirements limit most practical electroosmotically driven flows in microchannels to small Reynolds numbers; therefore to simplify eq 2a then we ignore transient and convective terms and limit ourselves to cases where $Re < 0.1$. F_e represents the nondimensional electroosmotic body force give by

$$F_e = \left(\frac{\epsilon_w \phi_{max} k_b T}{zew\eta v_{eo}}\right)[\tilde{\nabla}^2\Psi\cdot\tilde{\nabla}\Phi] \qquad (2c)$$

where Ψ represents the nondimensional EDL field strength ($\Psi = z\psi e/k_b T$, where k_b is the Boltzmann constant, T is the absolute temperature, e is the charge of an electron, and z is the ionic valence), Φ is the nondimensional applied electric field strength ($\Phi = \phi/\phi_{max}$, where ϕ_{max} is the maximum applied voltage) and the $\sim$ symbol over the ∇ operator indicates the gradient with respect to the nondimensional coordinates ($X = x/w$, $Y = y/w$, and $Z = z/w$).

As is apparent from eq 2c full evaluation of the electroosmotic body force requires a description of both Ψ and Φ, which can be given by eq 3 and eq 4 respectively

$$\tilde{\nabla}^2\Psi - K^2 \sinh(\Psi) = 0 \qquad (3)$$

$$\tilde{\nabla}^2\Phi = 0 \qquad (4)$$

where K is the nondimensional double layer thickness. ($K = \kappa w$, where κ is the Debye−Huckel parameter, given by $\kappa = (2n_o z^2 e^2/\epsilon_w k_b T)^{1/2}$ where n_o is the bulk ionic concentration of the aqueous medium. $1/\kappa$ is usually referred to as the characteristic thickness of the double layer as shown in Figure 1.) Inherent in eqs 3 and 4 are a few assumption that are worth discussing. The description of the applied electric field by the homogeneous Poisson equation is a simplification valid only in cases where the bulk conductivity of the aqueous solution does not change significantly within the channel (for a more general formulation see Ermakov et al.[18]). In the majority of cases of fluidic transport in microchip devices the species of interest are transported in a buffer solution with an ionic concentration 100 times greater than that of the species.[18] In these cases the buffer conductivity is assumed to dominate and thus remains constant, independent of the local species concentration. This assumption is also applicable to eq 3 that has been derived for a symmetric ionic species with concentration n_o. n_o is referred to the buffer concentration and the contribution of the more dilute species of interest has been ignored. By decoupling the equations for the EDL and applied electric field, it has been assumed that the charge distribution near the wall is unaffected by the externally applied field. Along the same lines, the description of the EDL field by the nonlinear Poisson−Boltzmann equation assumes that the double layer distribution is also undisturbed by external convective influences. As is discussed by Saville[22] these assumptions are generally valid as long as the double layer thickness is not large, or equivalently the ionic concentration of the solution is not very low and the flow remains in the limit of low Re.

Numerical modeling of electrokinetic flow and species mixing in a T-shaped mixer is complicated by the simultaneous presence of three separate length scales: the mixing channel length (mm), the channel cross sectional dimensions (μm), and the double layer thickness, $1/\kappa$ (nm), which we will refer to as L_1, L_2, and L_3, respectively. In general the amount of computational time and memory required to fully capture the complete solution on all three length scales would make such a problem nearly intractable. Since the channel length and cross sectional dimensions are required to fully define the problem (L_1, L_2), most previous studies[18−20] have resolved this problem by either eliminating or increasing the length scale associated with the double layer thickness (L_3). Both Bianchi et al.[19] and Patankar et al.[20] accomplished this by artificially inflating the double layer thickness to bring its length scale nearer that of the channel dimensions. This allowed them to fully solve for the EDL field, calculate the electroosmotic forcing term, and incorporate it into the Navier−Stokes equation without any further simplification. It did however not fully eliminate the third length scale, and considerable mesh refinement was still required near the channel wall. In these cases this approach was tractable largely because the geometries were selected such that the channel length (L_1) was not as large as that examined here. In a different approach Ermakov et al.[18] set $F_e = 0$ in eq 2a and applied a slip boundary condition at the channel, v_{eo} from eq 1. By this method the double layer length scale (L_3) is completely eliminated from the solution domain, and a description of the double layer region is no longer required. A similar slip condition approach was used by Stroock et al.[8] in their simulations of electrokinetically induced circulating flows. In both cases excellent agreement was obtained with experimental results. In this work, the large mixing channel length and the extension to 3D mixing require that we follow the slip condition approach.

As is shown in Figure 2, we consider the mixing of equal portions of two buffer solutions, one of which is contains a concentration, c_o, of a species of interest. Species transport by electrokinetic means is accomplished by three mechanisms, convection, diffusion, and electrophoresis,

(21) Erickson, D.; Li, D. Submitted for publication in *Int. J. Heat Mass Trans.*

(22) Saville, D. A. *Annu. Rev. Fluid Mech.* **1977**, *9*, 321−337.

and can be described by eq 5[18]

$$Pe\left[\frac{\partial C}{\partial \tau} + \tilde{\nabla}\cdot(C(V + V_{ep}))\right] = \tilde{\nabla}^2 C \qquad (5)$$

where C is the nondimensional species concentration ($C = c/c_o$, where c_o is original concentration of the interested species in the buffer solution), Pe is the Péclet number ($Pe = v_{eo}w/D$, where D is the diffusion coefficient), and V_{ep} is the nondimensional electrophoretic velocity equal to v_{ep}/v_{eo}, where v_{ep} is given by eq 6

$$v_{ep} = \mu_{ep}\nabla\phi \qquad (6)$$

and μ_{ep} is the electrophoretic mobility. In our study we are interested in the steady-state solution, thus the transient term in eq 5 can be ignored.

Before continuing, it would be useful to clarify the relationship between the three different velocities discussed above: the electroosmotic velocity V_{eo} (eq 1), the bulk flow velocity V (eqs 2a and 2b), and the electrophoretic velocity V_{ep} (eq 6). As shown in Figure 1, V_{eo}, is the induced velocity at the edge of the double layer caused by the application of the external electric field. As described above this quantity is used as a boundary condition on the Navier−Stokes equations, which are then used to determine the local velocity of the bulk flow at each point, V. While velocity at the boundary, V_{eo}, governs the magnitude V, it is important to distinguish between these two quantities. The velocity V_{ep}, represents the mobility of the species in the applied electric field. For a neutral species the electrophoretic velocity is zero, leaving V as the only velocity in eq 5. A charged species however will be attracted to either the positive or negative electrode, depending on the sign of the charge, at a speed described by V_{ep}. In such a case the total species convection is described by the superposition of V and V_{ep} as shown in eq 5. For further information on species mobility and its contribution to the convection diffusion equation (or more precisely the Nernst−Planck equation), the reader is referred to the texts by Lyklema.[23,24]

B. Solution Domain, Additional Boundary Conditions, and Numerical Method. In all simulations a square geometry was used with the depth equaling the width of the channel, w, and for consistency the arm length, L_{arm}, was also assigned the value of w. The length of the mixing channel, L_{mix}, was dictated by that required to obtain a uniform concentration (i.e., fully mixed) at the outflow boundary. Depending on the simulation conditions, this required L_{mix} to be on the order of 200 times the channel width.

The applied electric field strength, eq 4, was solved subject to $\Phi = 1$ at the inflow boundaries, $\Phi = 0$ at the outflow, and insulation conditions along the channel walls. The hydrodynamic influence of the surface heterogeneities was introduced into the solution through the electroosmotic slip boundary conditions that were applied on all surfaces and used to solve eqs 2a and 2b simultaneously. Zero gradient inflow conditions were applied at the two inlet regions ($\partial V_x/\partial X = 0$, $V_y = 0$, $V_z = 0$) and similarly at the outflow boundary ($V_x = 0$, $\partial V_y/\partial Z = 0$, $V_z = 0$). As mentioned above we consider the case of a stream with species concentration $c = c_o$ mixing with a buffer, thus we assign $C = 1$ to the right inlet boundary (inlet stream 2) and $C = 0$ to the left inlet (inlet stream 1).

Equations 2a, 2b, 4, and 5 were all solved over the computational domain via the finite element method[25] using 27-noded triquadratic brick elements for Φ, V, and C and 8-noded trilinear brick elements for pressure, using an in-house-written code. Through extensive numerical experimentation, these higher order elements were found to be much more stable, especially when applied to the convection−diffusion equation, eq 5, than their lower order counterparts and were thus implemented here. In all cases the discretized systems of equations were solved using a quasi-minimal residual method solver and were preconditioned using an incomplete LU factorization. In addition to testing the flow code against standard test problems the electrokinetic transport simulations were validated against the numerical/experimental results published by Ermakov et al.[18]

III. Results and Discussion

As eluded to in the preceding sections, the purpose of this study is to investigate the formation of electroosmotically induced circulation regions near surface heterogeneities in a T-shaped micromixer and to determine the influence of these regions on the mixing effectiveness. To begin we consider a standard test case of a channel 50 μm in width and 50 μm in depth, an applied voltage of $\phi_{app} = 500$ V/cm ($\phi_{app} = \phi_{max}/(L_{mix} + L_{arm})$), and a mixing channel length of 15 mm. These conditions are applied to all simulations unless otherwise specified. Consistent with the values used by Ermakov et al.,[18] we choose a homogeneous electroosmotic mobility of 4.0×10^{-8} m^2/(V s), corresponding to a homogeneous ζ potential of -42 mV. In Figure 3 we compare the mid-plane flow field near the T-intersection generated from (a) the homogeneous case, with that (b) caused by the presence of a series of six symmetrically distributed heterogeneous patches on the left and right channel walls and (c) a series of offset patches also located on the left and right walls, respectively. For clarity the heterogeneous regions are marked as the crosshatched regions in this and all subsequent figures. A ζ-potential of $\zeta = +42$ mV was assumed for the heterogeneous patches. As expected both diagrams b and c of Figure 3 do exhibit regions of local flow circulation near these heterogeneous patches; however their respective effects on the overall flow fields are dramatically different. In Figure 3b it is apparent that the symmetric circulation regions force the bulk flow streamlines to converge into a narrow stream through the middle of the channel. The curved streamlines shown in Figure 3c show the more tortuous path through which the bulk flow passes as a result of the offset, nonsymmetric circulation regions.

Figure 4 compares both the 3D and channel midplane concentration profiles for the three heterogeneous arrangements shown in Figure 3. In all these figures a neutral mixing species (i.e., $\mu_{ep} = 0$, thereby ignoring any electrophoretic transport for the time being) with a diffusion coefficient $D = 3 \times 10^{-10}$ m^2/s is considered. As expected both symmetric flow fields discussed above have yielded symmetric concentration profiles as shown in Figure 4,b. While mixing in the homogeneous case is purely diffusive in nature, the presence of the symmetric circulation regions, Figure 4b, enables enhanced mixing by two mechanisms, first through convective means by circulating a portion of the mixed downstream fluid to the unmixed

(23) Lyklema, J. *Fundamentals of Interface and Colloid Science, Volume 1*: *Fundamentals*; Academic Press: San Diego, CA, 1991.

(24) Lyklema, J. *Fundamentals of Interface and Colloid Science, Volume 2*: *Solid−Liquid Interfaces*; Academic Press: San Diego, CA, 1995.

(25) Heinrich, J. C.; Pepper, D. W. *Intermediate Finite Element Method*; Taylor & Francis: Philadelphia, PA, 1999.

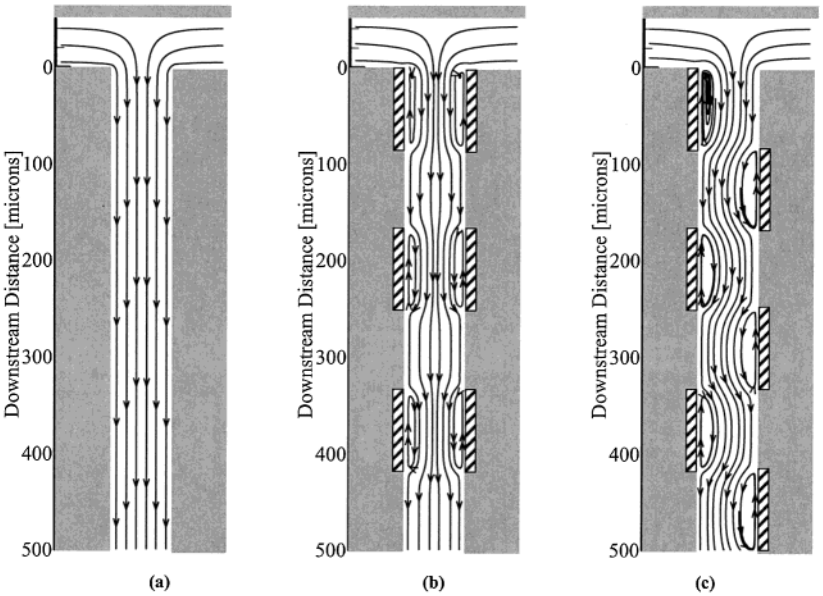

Figure 3. Electroosmotic streamlines at the midplane of a 50 μm T-shaped micromixer for the (a) homogeneous case with $\zeta = -42$ mV, (b) heterogeneous case with six symmetrically distributed heterogeneous patches on the left and right channel walls, and (c) heterogeneous case with six offset patches on the left and right channel walls. All heterogeneous patches are represented by the crosshatched regions and have a $\zeta = +42$ mV. The applied voltage is $\phi_{app} = 500$ V/cm.

upstream region and second by forcing the bulk flow through a significantly narrower region, as shown by the convergence of the streamlines in Figure 3b. In this second mechanism, the local concentration gradients are increased leading to a greater diffusive flux along the channel width (*x*-axis in Figure 2), *N*, given by eq 7

$$N = D\frac{\partial C}{\partial x} = O\left(D\frac{\Delta C}{L_{diff}}\right) \tag{7}$$

where L_{diff} is the diffusion length scale. In the homogeneous case L_{diff} is equivalent to the channel width, *w*. For the case shown in Figure 3b however the heterogeneous regions force the bulk flow to pass through a narrower region, resulting in $L_{diff} < w$ and thereby increasing *N*. This enhancement of the concentration gradients is apparent from parts a and b of Figure 5, which compare the cross sectional concentration contours for these two cases at distances of 200 μm (top plot) and 750 μm (bottom plot) downstream from the intersection. At 200 μm downstream (within the heterogeneous region), the convergence of the bulk flow into a narrow stream has led to the greater concentration gradients, as compared to Figure 5a, within this narrow band at the center of the channel. This results in much stronger diffusion and a more uniform species distribution further downstream, and thus better mixing, as shown in the 750 μm downstream contour plots.

In Figure 4c the convective effects on the local species concentration is apparent from the concentration contours generated for the nonsymmetrical, offset patch arrangement. In Figure 5c the influence of these offset patches on the mixing is apparent again leading to a similar enhancements in the concentration gradients at the 200 μm downstream point and a more uniform distribution at 750 μm downstream. In this case however the concentration distribution is no longer symmetric about the center axis.

A. Influence of the Heterogeneous ζ-Potential. In the previous section we have demonstrated qualitatively how the presence of heterogeneous regions can enhance the mixing process in a T-shaped micromixer. To quantify the degree of enhanced mixing, we introduce a mixing efficiency, ϵ, similar to that used by Jeon et al.,[13] given by eq 8

$$\epsilon(y) = \left(1 - \frac{\int_A |c - c_\infty|\, dA}{\int_A |c_0 - c_\infty|\, dA}\right) \times 100\% \tag{8}$$

where *c* is the cross sectional concentration profile at a distance *y* downstream and c_∞ and c_0 are the concentration profiles associated with a completely mixed and completely unmixed states, respectively. A fully mixed state therefore would have a 100% mixing efficiency, while the unmixed state would have a 0% mixing efficiency.

Figure 6 demonstrates the influence of the ζ-potential of the heterogeneous region on the mixing efficiency for a 50 μm mixing channel with a 500 μm long heterogeneous region on all four channel faces (beginning at the intersection) for an electrically neutral species with $D = 3 \times 10^{-10}$ m^2/s. The applied electric field strength is $\phi_{app} = 500$ V/cm and the total mixing channel length is 15 mm. As in the previous cases the channel has a ζ-potential of -42 mV in all regions outside the heterogeneous patches. From Figure 6 it is apparent that in all cases the introduction of heterogeneous patches does lead to an increase in the mixing efficiency over the homogeneous case. The largest improvement comes from the oppositely charged patch arrangement ($\zeta = +42$ mV) where the length to achieve 50% mixing efficiency is decreased by nearly 30% (390 μm vs 550 μm). Similarly, the length to achieve 70% mixing is also decreased by 30% (820 μm vs 1230 μm).

In general it was observed that the circulation regions shown in parts b and c of Figure 3 were only present when the heterogeneous ζ-potential was of opposite sign to that of the homogeneous surface. Additionally the size of the circulation regions was observed to increase as the magnitude of the heterogeneous ζ-potential was increased. Referring back to Figures 3, 4, and 5 then, larger circulation regions would force the bulk flow to pass through a narrower region leading to shorter local diffusion

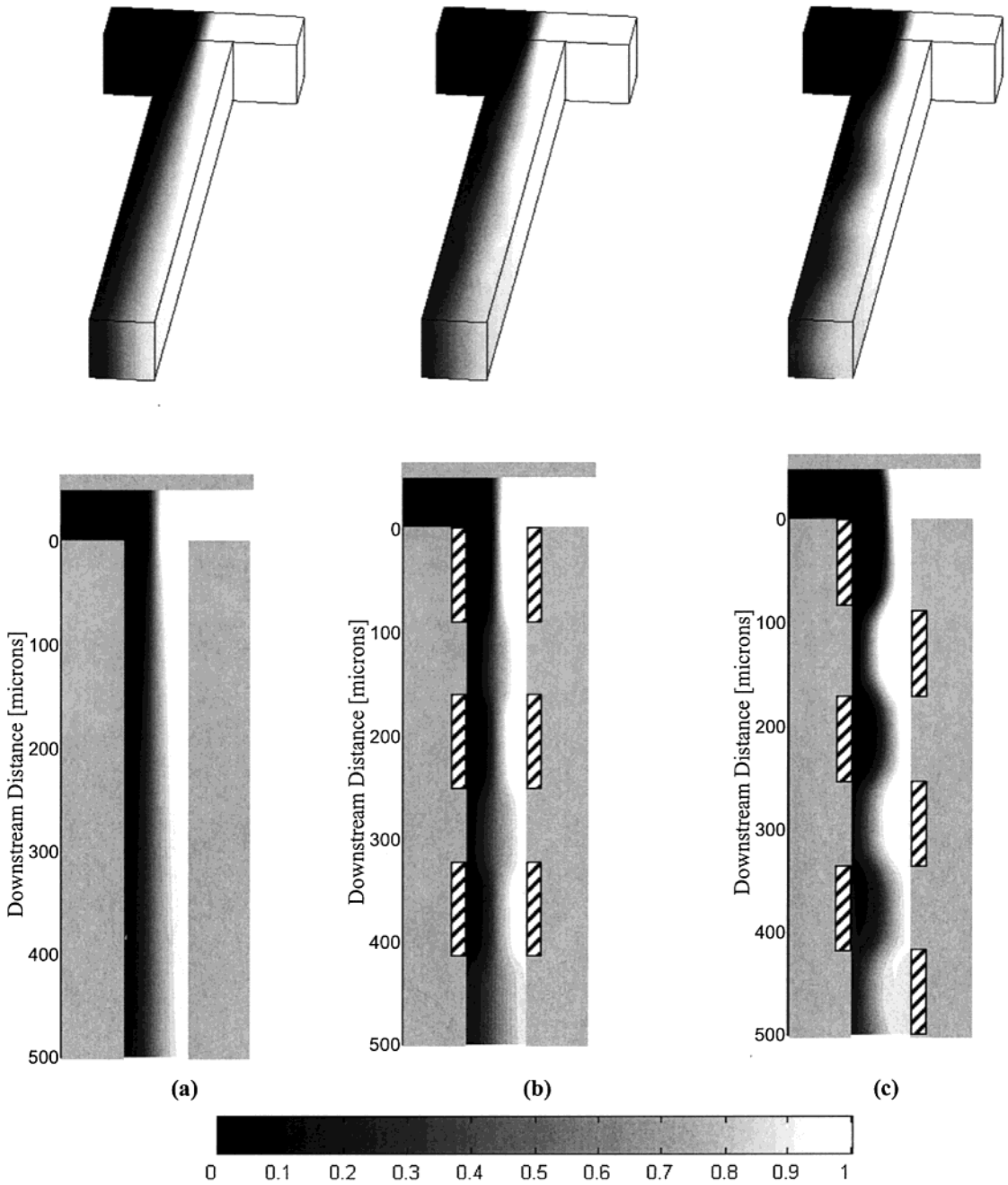

Figure 4. 3D species concentration contours (upper image) the midplane contours (lower image) for the 50 μm T-shaped micromixer resulting from the flow fields shown in Figure 3: (a) homogeneous case; (b) heterogeneous case with symmetrically distributed heterogeneous patches; (c) heterogeneous case with offset patches. Species diffusivity is 3×10^{-10} m^2/s and zero electrophoretic mobility is assumed.

length and thus by eq 6 enhanced mixing. Despite the lack of circulation zones in the $\zeta = -21$ mV and $\zeta = 0$ mV cases, a slight convergence of the flow streamlines to a narrower region at the center of the channel, caused by the localized slowing of the velocity field near the channel walls, was observed and proved to be sufficient to provide some degree of enhanced mixing.

In Figure 6 it can also be seen that all cases exhibit an approximate step change in the mixing efficiency immediately after the heterogeneous region. This occurs as a result of the higher concentration gradients in the center of the channel making the mixing efficiency appear artificially low. Referring back to Figure 5b it can be seen that within the heterogeneous region the gradients in the concentration profile occur over a relatively thin band in the middle of the channel cross section, leading to the improved mixing as discussed above. Outside of this narrow band the species appear nearly unmixed resulting in an artificially low mixing efficiency. When the streamlines diverge rapidly at the termination of the heterogeneous patch, see Figure 3b, the concentration gradients are expanded to encompass the full channel width, as is shown in the lower image in Figure 5b, leading to the observed rapid change in the mixing efficiency. This effect is also well demonstrated on the 2D image in Figure 4b where the expansion of the concentration gradients after the termination of a heterogeneous patch and the contraction at the beginning of the heterogeneous patch are both well shown.

Also in Figure 6 it can be observed that the $\zeta = +42$ mV case has a significantly higher mixing efficiency at the intersection (downstream distance = 0 μm) than the other

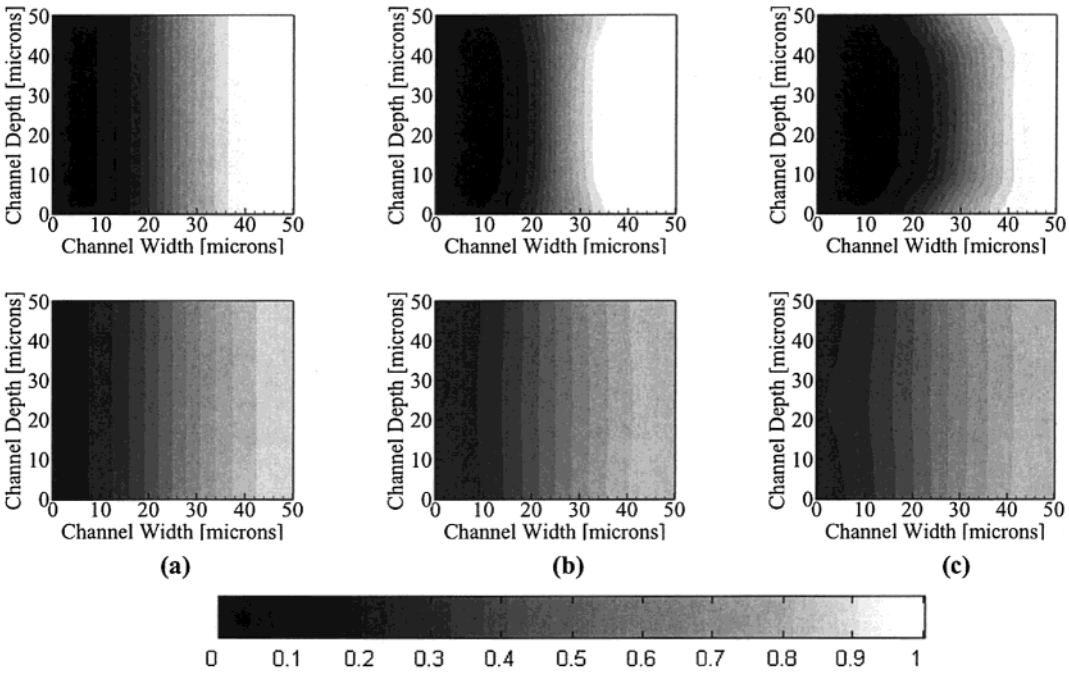

Figure 5. Species concentration contours in the cross section of the T-shaped micromixer at 200 μm downstream (upper image) and 750 μm downstream (lower image) for the three cases shown at Figure 4: (a) homogeneous case; (b) heterogeneous case with symmetrically distributed heterogeneous patches; (c) heterogeneous case with offset patches.

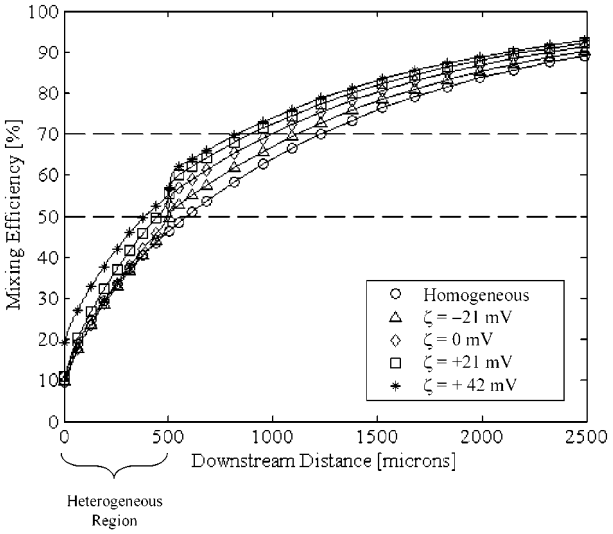

Figure 6. Effect of the heterogeneous patch ζ-potential on the mixing efficiency of a 50 μm T-shaped micromixer with ϕ_{app} = 500 V/cm. A single 500 μm patch on all four sides of the channel was used and the homogeneous ζ-potential is -42 mV. Species diffusivity is 3×10^{-10} m^2/s, and zero electrophoretic mobility is assumed.

cases. This immediate enhancement is a result of stronger circulation zones convecting a greater portion of the mixed downstream solution upstream to the entrance. Interestingly however this effect appears to be localized to the heterogeneous region, as the absolute difference between the mixing efficiencies for the $\zeta = +42$ mV and $\zeta = +21$ mV cases outside the heterogeneous region is no greater than one would expect due to the enhanced concentration gradients (based on the trend from the lower ζ potential simulations). Therefore, while the recirculation mechanism does provide significant improvement of the initial mixing efficiency (at the beginning of the heterogeneous region), it appears as though the enhanced concentration gradients are the dominant mechanism for overall enhanced mixing.

B. Influence of Heterogeneous Patch Size and Arrangement. Figure 7 shows the influence of the heterogeneous patch size on the mixing efficiency for two different applied voltages: (a) $\phi_{app} = 500$ V/cm and (b) $\phi_{app} = 200$ V/cm. As before we consider the case of a single heterogeneous patch with $\zeta = +42$ mV on all four sides of a homogeneous surface with $\zeta = -42$ mV, a 50 μm by 50 μm cross section channel, and $D = 3 \times 10^{-10}$ m^2/s. Apparent in both cases is that the larger patches, exposing the solution to the enhanced concentration gradients for a longer time, will increase the overall mixing efficiency. It is not surprising that as the ϕ_{app} is decreased, resulting in slower flow in the lengthwise direction and allowing greater time for diffusion, the mixing efficiency is improved. Additionally the longer retention time in the heterogeneous region for the lower voltage case also serves to improve the effectiveness of the heterogeneous region, reducing the required mixing length to attain both 50% and 70% mixing efficiency by about 70%, compared with 30% for the larger applied voltage case.

To investigate the effects of patch distribution, we consider the two general arrangements shown in Figure 3b (symmetric) and Figure 3c (offset) and the same transport conditions as those detailed above with $\phi_{app} = 500$ V/cm. We consider both four-patch and six-patch arrangements (Figure 3b and Figure 3c represent the six-patch arrangement) with the patch sizes being adjusted so that in each case a total of 250 μm of heterogeneous surface is spread out over the first 500 μm distance downstream of the intersection on both the left and right sides (e.g., in Figure 3c there are three 83.3 μm patches on the right surface for a total of 250 μm of heterogeneous surface). The resulting mixing efficiencies for these cases are compared in Figure 8. In Figure 8 it is apparent that, in terms of the mixing efficiency outside the heterogeneous region, for both cases there is almost no difference between the four- and six-patch arrangements. In addition, very little difference between the symmetric and offset dis-

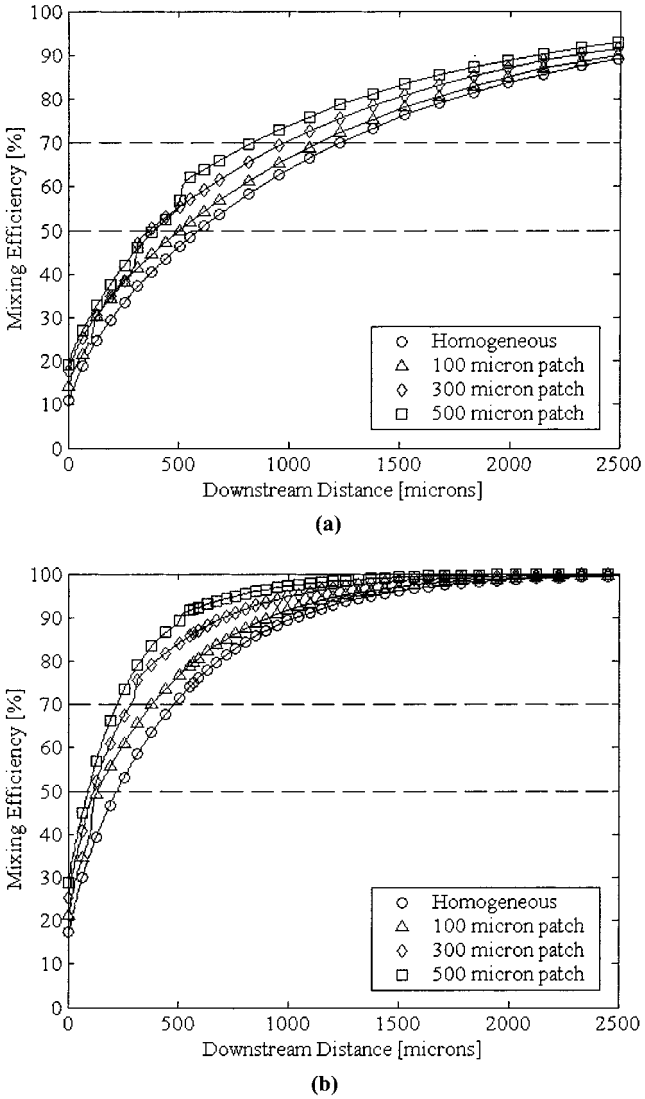

Figure 7. Effect of the heterogeneous patch size on the mixing efficiency of a 50 μm T-shaped micromixer with (a) $\phi_{app} = 500$ V/cm and (b) $\phi_{app} = 200$ V/cm. A single patch on all four sides of the channel with $\zeta = +42$ mV was used and the homogeneous ζ-potential is -42 mV. Species diffusivity is 3×10^{-10} m^2/s and zero electrophoretic mobility is assumed.

tributions is observed, suggesting that mixing efficiency is more a function of patch size, rather than the arrangement.

The most striking feature of the results displayed in Figure 8 is the large oscillation in the mixing efficiency within the heterogeneous region, most significantly for the symmetric patch case. As was discussed in section III.A, near step changes in the mixing efficiency are observed at the termination of a heterogeneous patch due to the expansion of the concentration gradients. Referring back to Figure 4b, it is apparent that as the flow passes through multiple heterogeneous regions the concentration gradients experience numerous expansion and contraction zones resulting in the observed oscillations in the mixing efficiency. Since the concentration gradients are compressed into a significantly smaller region than is observed in the homogeneous case, as is shown in the upper images of Figure 5, it is not surprising that in some cases the mixing efficiency in the heterogeneous region drops below that of the homogeneous channel.

C. Influence of Channel Size. Figure 9 compares the mixing efficiency in a 50 μm $\times$ 50 μm channel with that

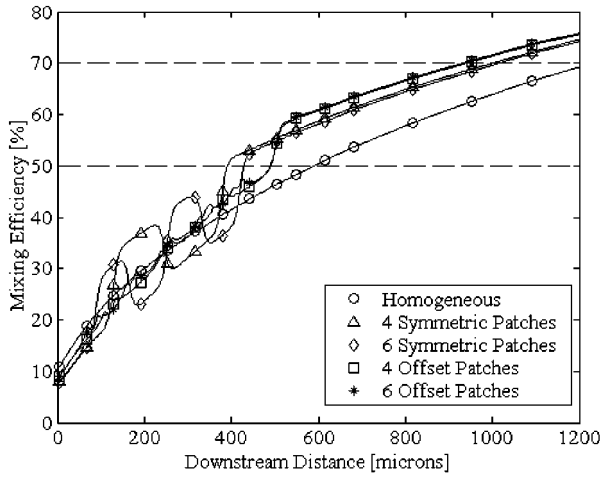

Figure 8. Influence of the heterogeneous patch arrangement on the mixing efficiency of a 50 μm T-shaped micromixer with $\phi_{app} = 500$ V/cm. The symmetric and offset patch arrangements are as shown in Figure 3b and Figure 3c, respectively (six-patch arrangement shown in both cases). The homogeneous ζ-potential is -42 mV and all heterogeneous patches have $\zeta = +42$ mV. Species diffusivity is 3×10^{-10} m^2/s, and zero electrophoretic mobility is assumed.

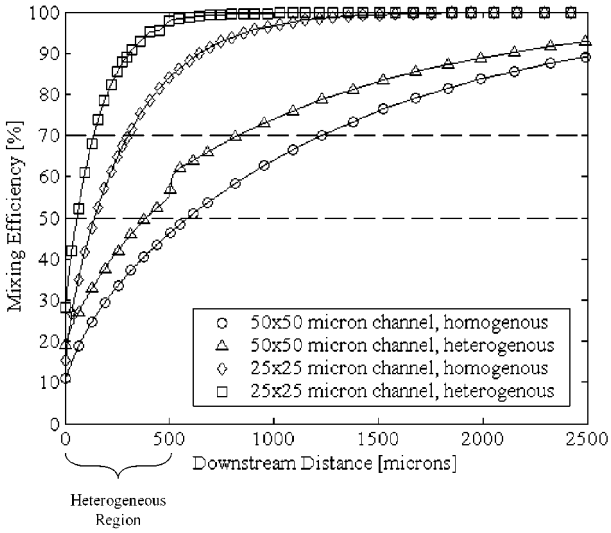

Figure 9. Effect of channel size on the mixing efficiency for both homogeneous and heterogeneous cases with $\phi_{app} = 500$ V/cm. For the heterogeneous cases a single 500 μm patch on all four sides of the channel was assumed with $\zeta = +42$ mV and a homogeneous ζ-potential of -42 mV was used. Species diffusivity is 3×10^{-10} m^2/s and zero electrophoretic mobility is assumed.

in a 25 μm $\times$ 25 μm channel for both the homogeneous and heterogeneous cases. As expected the smaller diffusion length, L_{diff} from eq 7, in the 25 μm channel leads to an increased mixing efficiency over that exhibited by the 50 μm homogeneous channel. Also in Figure 9, it is apparent that the influence of the heterogeneous patches is significantly greater for the 25 μm channel, with 50% reductions in L_{mix} at both the 50% and 70% mixing efficiency points (compared to 30% for the larger channel) and resulting in nearly complete mixing at only 500 μm distance downstream.

D. Influence of Species Diffusivity and Electrophoretic Mobility. In the previous sections we have confined ourselves to analysis using electrically neutral molecules, where the electrophoretic transport component in eq 5 has been neglected, with constant diffusion coefficient of $D = 3 \times 10^{-10}$ m^2/s. In this section we seek

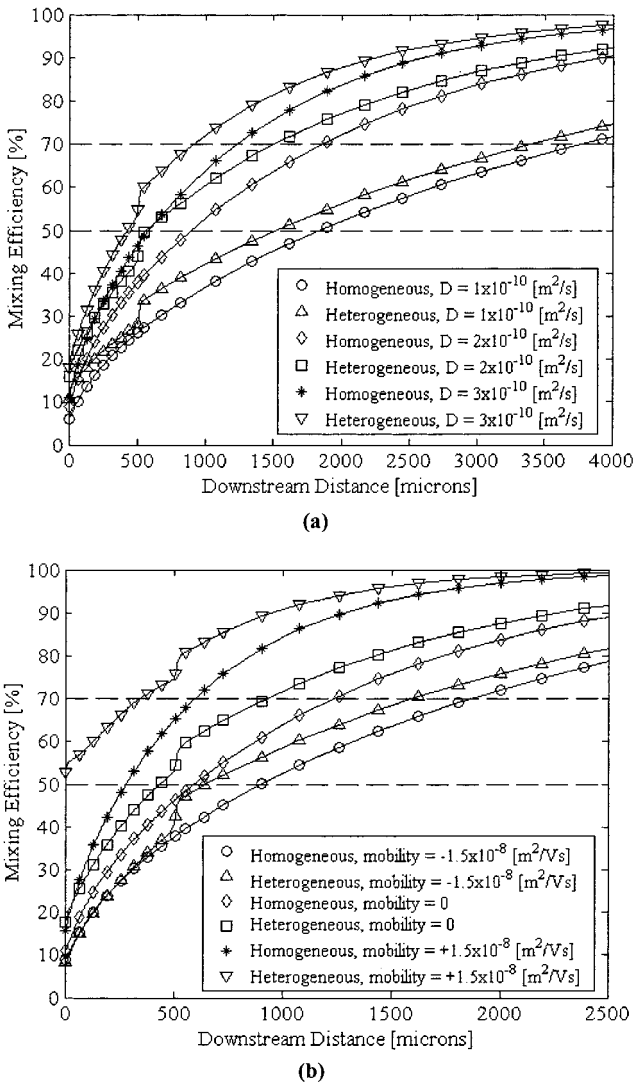

Figure 10. Influence of (a) species diffusivity and (b) electrophoretic mobility on the mixing efficiency in a 50 μm channel for both homogeneous and heterogeneous cases with $\phi_{app} = 500$ V/cm. For the heterogeneous cases a single 500 μm patch on all four sides of the channel was assumed with $\zeta = +42$ mV and a homogeneous ζ-potential of -42 mV was used.

to understand how the enhanced mixing efficiency is affected by the diffusivity and electrophoretic mobility of the mixing species. In Figure 10 we reexamine the standard test case of a 50 μm $\times$ 50 μm channel and a single heterogeneous region with $\zeta = +42$ mV on all four sides of the first 500 μm of the mixing channel. Figure 10a shows the effect of species diffusivity by examining diffusion coefficients ranging from 1×10^{-10} to 3×10^{-10} m^2/s. As in the previous cases a near step change in the mixing efficiency is observed at the termination of the heterogeneous region (both parts a and b of Figure 10) due to the expansion of the channel concentration gradients as discussed in detail in section III.A. From eq 7 it is apparent that for lower D values the species flux will decrease and thus the observed lower mixing efficiency should result. This is clearly observed in Figure 10a where significantly lower mixing efficiencies are observed for the $D = 1 \times 10^{-10}$ m^2/s case for both homogeneous and heterogeneous channels. Also apparent in Figure 10a is that while in all cases the introduction of surface heterogeneities does improve the mixing efficiency, the absolute reduction in the mixing length is approximately equal for all pairs. This suggests that the effects of a higher diffusion coefficient on the mixing efficiency are neither enhanced nor degraded due to the presence surface heterogeneity.

Figure 10b illustrates the influence of the electrophoretic mobility on the mixing in both homogeneous and heterogeneous channels, for the identical simulation conditions listed above and $D = 3 \times 10^{-10}$ m^2/s. Since a negative electrophoretic mobility increases the magnitude of the convection term in eq 5 (since V and V_{ep} will be in the same direction) whereas a positive mobility tends to reduce its magnitude, it would be expected that at a fixed downstream distance the mixing efficiency of the later of these would be considerably higher than that of the former. This is well demonstrated in Figure 10b where both heterogeneous and homogeneous surfaces exhibit significant increases in the mixing efficiency as μ_{ep} is increased from -1.5×10^{-8} to $+1.5 \times 10^{-8}$ m^2/(V s). Of interest in this plot is the significant increase in the initial mixing efficiency exhibited by the positive mobility case with the heterogeneous region. This significant initial enhancement is a result of the superposition of the electrophoretic and electroosmotic transport in the heterogeneous region near the wall (where the local flow direction is opposite that of the bulk flow) allowing a greater circulation of downstream ions into the unmixed initial solution.

E. Brief Comments on the Practical Aspects. In the preceding sections we have shown through numerical simulations how the presence of electrokinetically heterogeneous patches can significantly enhance the efficiency of a T-shaped mixer. Before concluding however, a brief discussion on the practical aspects of implementing such a technique is warranted. In general a variety of techniques are available for creating such heterogeneous patches, the most common of which is likely micro-contact printing, which would fall into the category of soft lithography. As mentioned earlier, Stroock et al.[8] were able to generate oppositely charged, stable heterogeneous patches (using a soft lithography technique) in an electrolyte solution and directly observe these circulation zones. Of note is the fact that the results presented in Figure 6 suggest that precise control over the exact values of ζ-potential is not required, as all degrees of heterogeneity will lead to at least some enhanced mixing. It should also be noted that the adsorption of the transported species, such as proteins or other bioparticles, on the channel wall is likely to cause some fouling and change the effective ζ-potential; the efficiency of the heterogeneous surface technique is likely to be significantly reduced.

IV. Summary and Conclusions

For low Reynolds number electroosmotically driven flows in microfluidic devices, species mixing is inherently diffusion dominated, resulting in poor mixing efficiency or requiring long transport distances and retention time. In this study the effects of surface electrokinetic heterogeneity on the electroosmotic flow and mixing efficiency of a T-shaped micromixer was investigated through 3D numerical simulations.

While all cases of surface heterogeneity were shown to enhance species mixing, the greatest improvements were found when the ζ-potential of the heterogeneous surface was of opposite sign to that of the homogeneous surface, resulting in localized circulation zones within the bulk flow field. The local flow circulation enhances the mixing by, first, convection means by circulating a portion of the mixed downstream fluid to the unmixed upstream region and, second, forcing the bulk flow through a significantly narrower region to increase the local concentration gradients.

For a fixed ζ-potential, the length of the heterogeneous patch was found to be the most important factor while the patch distribution had only marginal effects on the mixing efficiency. In general the mixing efficiency improvement by decreasing the applied voltage and the channel size will be enhanced through the introduction of surface heterogeneity, in some cases resulting in a 70% reduction in the required mixing length. The combined effect of the heterogeneous patch and a positive electrophoretic mobility was shown to be significant in enhancing the initial mixing efficiency at the T-intersection.

Acknowledgment. The authors are thankful for the financial support of the Natural Sciences and Engineering Research Council through a scholarship to David Erickson and through a research grant to D. Li. Additionally the authors would like to acknowledge Professor Dan Kwok at the University of Alberta and Dr. Carsten Werner at the Institute for Polymer Research Dresden for their helpful discussions regarding the creation of heterogeneous surfaces.

LA015646Z